High-Resolution Three-Dimensional Structural Data Quantify the Impact of Photoinhibition on Long-Term Carbon Gain in Wheat Canopies in the Field[1][OPEN]

Alexandra J. Burgess[2], Renata Retkute[2], Michael P. Pound, John Foulkes, Simon P. Preston, Oliver E. Jensen, Tony P. Pridmore, and Erik H. Murchie*

Division of Plant and Crop Sciences, School of Biosciences, University of Nottingham, Sutton Bonington LE12 5RD, United Kingdom (A.J.B., R.R., M.P.P., J.F., E.H.M.); School of Mathematical Sciences, University of Nottingham, Nottingham NG7 2RD, United Kingdom (R.R., S.P.P.); School of Mathematics, University of Manchester, Manchester M13 9PL, United Kingdom (O.E.J.); and School of Computer Science, Jubilee Campus, University of Nottingham, Nottingham NG8 1BB, United Kingdom (T.P.P.)

ORCID IDs: 0000-0002-1621-6821 (A.J.B.); 0000-0002-3877-6440 (R.R.); 0000-0003-0172-6578 (O.E.J.); 0000-0002-7465-845X (E.H.M.).

Photoinhibition reduces photosynthetic productivity; however, it is difficult to quantify accurately in complex canopies partly because of a lack of high-resolution structural data on plant canopy architecture, which determines complex fluctuations of light in space and time. Here, we evaluate the effects of photoinhibition on long-term carbon gain (over 1 d) in three different wheat (*Triticum aestivum*) lines, which are architecturally diverse. We use a unique method for accurate digital three-dimensional reconstruction of canopies growing in the field. The reconstruction method captures unique architectural differences between lines, such as leaf angle, curvature, and leaf density, thus providing a sensitive method of evaluating the productivity of actual canopy structures that previously were difficult or impossible to obtain. We show that complex data on light distribution can be automatically obtained without conventional manual measurements. We use a mathematical model of photosynthesis parameterized by field data consisting of chlorophyll fluorescence, light response curves of carbon dioxide assimilation, and manual confirmation of canopy architecture and light attenuation. Model simulations show that photoinhibition alone can result in substantial reduction in carbon gain, but this is highly dependent on exact canopy architecture and the diurnal dynamics of photoinhibition. The use of such highly realistic canopy reconstructions also allows us to conclude that even a moderate change in leaf angle in upper layers of the wheat canopy led to a large increase in the number of leaves in a severely light-limited state.

Plant canopy characteristics result from several factors, including genetically determined patterns of development, environmental influence on key developmental events (such as cell division), and population density. This means that plant canopies, whether considered as single plants or at the community scale, are spatially complex, resulting in a heterogeneous light environment (Russell et al., 1989). Because photosynthetic rate is light intensity dependent, it is convenient to consider canopies as populations of leaves each consisting of surface areas with different characteristics and varying states of photosynthesis at any single time point. High-resolution three-dimensional (3D) representations of plant canopies have previously been difficult to obtain, and this has hampered predictions of canopy photosynthesis.

One of the consequences of canopy complexity is spatial and temporal variability in the onset of high light effects, such as photoinhibition. Here, we approach this problem by using unique techniques for high-resolution reconstruction of crop canopies in the field combined with an empirical model of photoinhibition. We consider photoinhibition as a light-dependent decline in the maximal quantum yield of photosynthesis, which can be monitored by a decrease

[1] This work was supported by Crops for the Future (project no. BioP1–006 to A.J.B.) and the Biotechnology and Biological Sciences Research Council (program funding no. BB/JOO3999/1 to the Centre for Plant Integrative Biology, R.R., M.P.P., S.P.P., O.E.J., T.P.P., E.H.M.; and Industrial Partnership Award no. BB/D008972/1 for wheat lines development).

[2] These authors contributed equally to the article.

* Address correspondence to erik.murchie@nottingham.ac.uk.

The author responsible for distribution of materials integral to the findings presented in this article in accordance with the policy described in the Instructions for Authors (www.plantphysiol.org) is: Erik H. Murchie (erik.murchie@nottingham.ac.uk).

E.H.M. conceived the experiment and coordinated the work; M.P.P. and T.P.P. developed the three dimensional reconstruction methodology that was adapted for this article; A.J.B. and R.R. developed the technique for reconstruction of whole canopies from individual plant reconstructions and the model for the impact of photoinhibition on canopy carbon gain; S.P.P., O.E.J., and R.R. applied the ray tracer to the reconstruction data and helped to devise the modeling approaches; E.H.M., A.J.B., and J.F. supervised the field measurements; J.F. designed the field trial and selected lines as being appropriate for the experiment based on architecture, photosynthesis, yield, and phenology; The first draft of the article was written by E.H.M., A.J.B., and R.R. with input on later drafts by M.P.P., S.P.P., and O.E.J.

[OPEN] Articles can be viewed without a subscription.
www.plantphysiol.org/cgi/doi/10.1104/pp.15.00722

in the chlorophyll fluorescence ratio of variable fluorescence (F_v) to maximal fluorescence (F_m; Powles, 1984; Long et al., 1994; Raven, 2011; Takahashi and Badger, 2011). The effect of photoinhibition on biomass production is not a unique concept, but very few techniques exist that are able to quantify its impact on long-term carbon gain at the canopy scale. The effect of photoinhibition on shaping parameters of the photosynthesis light response curve is already well characterized, and previous empirical models have looked at the effects of distorting such shaping parameters to empirically quantify values for reduction in carbon gain (Ögren and Sjöström, 1990; Werner et al., 2001; Zhu et al., 2004; Valladares et al., 2005).

The effect of photoinhibition on productivity is, to a large extent, dependent upon the capacity of a leaf to utilize incident photosynthetic photon flux density (PPFD) as described by the shape of the light response curve. Two shaping parameters determine a light response curve as defined by the nonrectangular hyperbola, namely the quantum yield of PSII (ϕ) and convexity (θ). The quantum yield (ϕ) describes the initial linear portion (under low light intensities) of the light response curve and defines the maximum efficiency with which light can be converted to fixed carbon. The primary effect of photoinhibition is the reduction in ϕ, which is important under low light conditions (Powles, 1984; Björkman and Demmig, 1987; Krause and Weis, 1991). Chlorophyll fluorescence measurements are often used to predict changes in ϕ for a given location within a canopy (as dark-adapted F_v/F_m), because this is a measurement of actual maximum yield of PSII. Gas exchange and oxygen evolution data indicate a near-equal (1:1) relationship between changes in F_v/F_m and changes in ϕ (Björkman and Demmig, 1987; Genty et al., 1989).

The convexity (θ) describes the curvature of a light response curve. The optical properties of leaves and acclimation of individual cells result in convexity values of around 0.85. Higher values of convexity ($\theta > 0.96$) can be found within unicellular algae (*Coccomyxa* spp.; Terashima and Saeki, 1985; Ögren and Sjöström, 1990; Evans et al., 1993; Leverenz, 1994).

Under conditions causing photoinhibition, a reduction in ϕ is often accompanied by a similar reduction in θ (Ögren and Sjöström, 1990; Leverenz, 1994). However, the main difference between the two parameters is that a reduction in ϕ will also reduce photosynthesis at intermediate light levels and not only under low light conditions. A reduction in both parameters is of particular importance under natural conditions, because light is thought to be a limiting resource to photosynthesis most of the time in a large number of environments (Long and Hällgren, 1985; Ort and Baker, 1988). The effect of photoinhibition on the light response curve can, therefore, be used to quantify its influence on long-term carbon gain by distorting the curve from a theoretical maximal value and calculating how the results differ from an undistorted curve.

Plant canopies represent an intriguing model for studies in photoinhibition, because for a given leaf, the 3D structure results in a pattern of light that frequently shifts between high and low irradiance as a result of solar movement and other factors, such as plant movement. Hence, photoinhibited leaves are frequently and momentarily exposed to a range of light intensities. Architecture, therefore, determines both the pattern of onset and the cost to productivity.

In previous studies, the reduction in F_v/F_m for a given leaf area was considered to be a function of the weighted PPFD exposure over the previous 6 h (Werner et al., 2001; Valladares et al., 2005) or the cumulative weighted PPFD over the previous 24 h (Zhu et al., 2004). We considered that this approach is not appropriate for comparisons between species and lineages where there may be variation in the quantum requirements for photoinhibition. There are known genotype-dependent differences in cereal species (Kasajima et al., 2011); therefore, we derived a scaling factor (SF) directly from F_v/F_m data taken in the field measured at different canopy levels.

As described above, the photosynthetic rate depends on the shape of the light response curve as well as local light conditions. Plants are complex 3D objects with a great variability in leaf size, shape, area, angle, curvature, twisting, and clumping. Moreover, plants show emergent morphological and physiological properties as a result of being grown as a community in the field and not as single plants in pots. Therefore, an accurate estimation of light environment inside a crop canopy requires both image-based high-resolution 3D plant reconstruction (Pound et al., 2014) and a ray-tracing algorithm (Song et al., 2013) from plants grown in realistic field scenarios. Combining the techniques allows prediction of a precise local PPFD at multiple positions for any given time point, which would be difficult to achieve using manual measurements. Furthermore, image-based reconstruction is more sensitive to small differences in plant architecture.

The empirical model that we propose uses the distortion of the light response curve from a maximal state parameterized by field-measured gas exchange and fluorescence data combined with detailed 3D structural data, where leaves are represented as a set of triangles. Ray tracing is used to assess the productivity of three field-grown wheat (*Triticum aestivum*) lines that contrast in plant architecture. Such a method can be used to assess the link between existing canopy architecture and carbon gain or could be used as a tool and platform for creating unique ideal plant types. Three wheat lines were selected for analysis in this study from an ongoing field trial at the University of Nottingham farm: cv Ashby, cv 32-129bc, and cv 23-74bc, which are referred to as the parent line, line 1, and line 2, respectively. We show that (1) variation in wheat canopy architecture measured using unique high-resolution 3D imaging affects both photoinhibition and canopy photosynthesis; (2) 3D reconstruction of entire canopies provides a convenient and accurate way of recovering descriptive

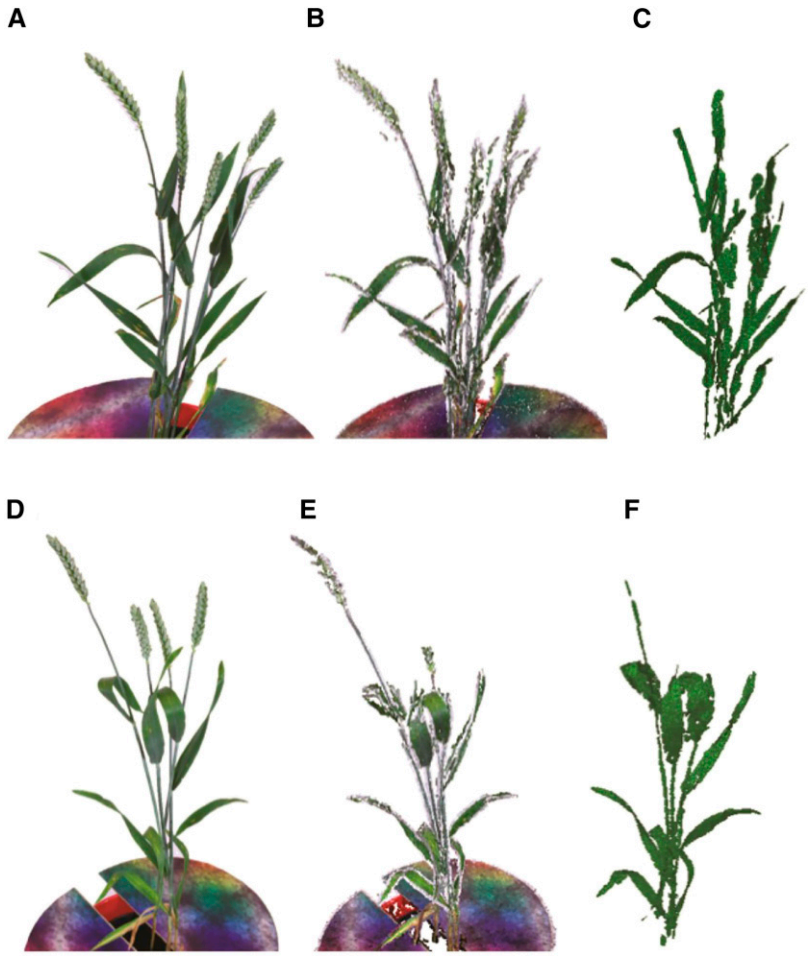

Figure 1. Stages of the reconstruction of a single plant from multiple color images. A and D, An example photograph of a wheat plant including the calibration target, from one viewpoint, of the parent line (upright leaves) and line 2 (more curled leaves), respectively. B and E, Point cloud reconstruction: the output when each set of images is run through VisualSFM (Wu, 2011). C and F, The final output mesh after using the reconstructor software (Pound et al., 2014) with the ears removed.

features used in canopy analysis for light interception and crop production that were previously difficult, if not impossible, to obtain; and (3) the distribution of light levels in contrasting canopies shows unique features in terms of the degree of saturation of photosynthesis according to canopy position.

RESULTS

Light Environment in Leaf Canopy

A major determinant of light environment in a leaf canopy is plant architecture, the general descriptors of which are leaf area, leaf inclination, and arrangement in space. Traditionally, theoretical work on photosynthesis considers canopies with randomly distributed leaves and leaf angles defined by a particular distribution to account for spatial heterogeneity (Werner et al., 2001; Zhu et al., 2004; Song et al., 2013). Our study is based on an accurate high-resolution digital reconstruction of real wheat canopy structure; therefore, it represents subtle features without the need to parameterize structural properties. Figure 1 shows two examples of the reconstruction process of single contrasting wheat plants, and Figure 2 shows the final three different reconstructed canopies (3- × 3-plant plots) designed to accurately represent the canopies from which each of the individual plant reconstructions was derived.

Clear visual differences between canopy geometrical measures of the three reconstructed canopies are apparent in Figure 2. The parent line has distinct upright leaves compared with the more curved and curled leaves of lines 1 and 2. This was confirmed by manual

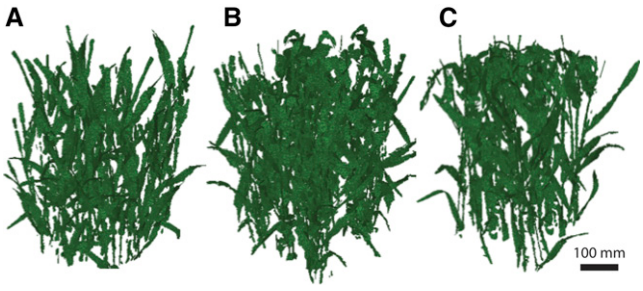

Figure 2. Wheat canopy reconstructions. All plots were made from single-plant reconstructions (as in Fig. 1), duplicated, randomly rotated, and spaced on a 3- × 3-plant grid. A, Parent line. B, Line 1. C, Line 2.

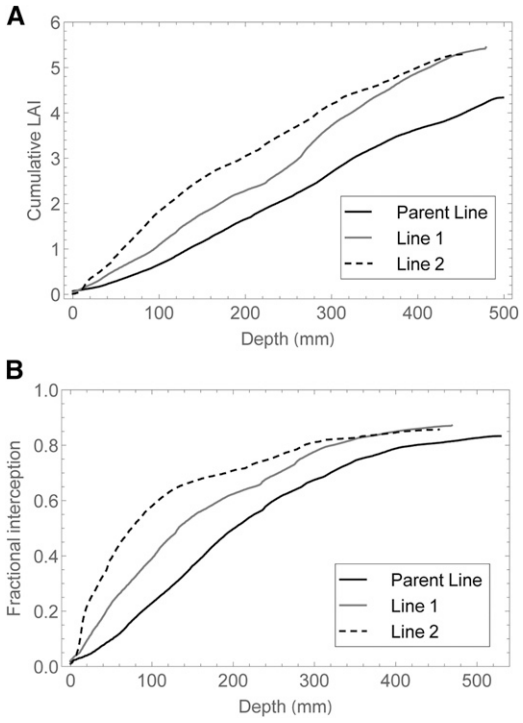

Figure 3. Properties of each canopy. A, cLAI (Eq. 1): the area of leaf material per unity ground as a function of depth through the canopy at 12 PM. B, Fractional interception (Eq. 3) as a function of depth in the canopy at 12 PM. Curves were calculated with step $\Delta d = 1$ mm.

measurements of leaf angle (as the angle with which the leaf subtends the stem; Supplemental Table S1). It was also confirmed by calculating the distributions of angles of the reconstructed leaf elements (also known as individual triangles; "Imaging and Ray Tracing") relative to the vertical axis (Supplemental Fig. S1).

We found substantial differences in vertical profiles of leaf material between the three canopies. We calculated the reconstructed leaf and stem area index to be 4.34 for the parent line, 5.33 for line 1, and 5.27 for line 2. Figure 3A shows cumulative leaf area index (cLAI) calculated as a function of depth using Equation 1 (see "Materials and Methods"). Although both lines 1 and 2 have a similar total canopy cLAI, line 2 accumulates more biomass at equivalent lower depths compared with line 1. The parent line has the lowest vertical distribution of biomass with depth. At the depth of 100 mm, cLAI is 0.66 for the parent line, 1.1 for line 1, and 1.8 for line 2.

Similar trends can be seen in plots indicating the fraction of solar incident radiation intercepted (F; Eq. 3; see "Materials and Methods") at midday, with each canopy exhibiting distinct dependence on depth (Fig. 3B). F accumulates more gradually in the parent line than in lines 1 and 2, with line 1 being intermediate between three canopies. For example, one-half of above-canopy PPFD is intercepted at the depths of 74 mm in line 2, 132 mm in line 1, and 201 mm in the parent line.

Simulations of the light environment show that the daily PPFD on average decreases with depth in all three plots, but the light environment has considerable spatial heterogeneity in PPFD at a fixed depth. Figure 4A shows a distribution of the logarithm of the ratio between PPFD absorbed at a point within a canopy and above-canopy PPFD at midday. The PPFD at any depth into the canopy can have a wide range of values, and Figure 4 shows that this variability increases with depth. Therefore, it is possible for a lower part of the canopy to have surface areas that receive higher PPFD than surface areas within upper parts of the canopy because of self-shading or shading by neighboring plants. This gives rise to the phenomenon termed sunflecks (Pearcy, 1990). Figure 4B takes this further, comparing the frequency of PPFD values according to the fraction of surface area in the top layer. Stark differences are seen between the lines, with the contrasting curled canopy (line 2) having a large proportion of leaf area in low light (below 150 μmol m^{-2} s^{-1}) compared with line 1 and the parent line. This high-resolution analysis is valuable when comparing light distributions against photosynthetic light response curves. Similar differences are present during the whole day (Supplemental Fig. S2).

Based on fractional interception as a function of cLAI, we calculated light extinction coefficients (k; Hirose, 2005) for the three canopies (Eq. 4; see "Materials and Methods"). Values of k are used in canopy analysis as a convenient way of mathematically describing the attenuation of light defined by architecture and dependent on the interaction between cLAI accumulation and fractional interception. The simulated values of k obtained are 0.40 for the parent line, 0.49 for line 1, and 0.61 for line 2. This corroborates findings from manually measured ceptometer data measured in the field (Fig. 5, line 2).

Incorporating Physiological Measurements into the Photoinhibition Model

An overview of the modeling process can be seen in Figure 6. Light response curves and F_v/F_m were measured at 12 PM at three levels within each canopy. The nonrectangular hyperbola given by Equation 5 (see "Materials and Methods") was fitted to experimental data to determine the maximum photosynthetic capacity, quantum use efficiency, and convexity. Measurements and fitted curves for line 1 are shown in Figure 7A. The maximum photosynthetic capacity decreased (Fig. 7A; Supplemental Fig. S3) and F_v/F_m increased (Fig. 7B) with the depth in the canopy. The differences between photosynthetic light response curves are typical of the canopy depth-dependent changes caused by light acclimation and leaf ageing (Murchie et al., 2002). Daily net photosynthesis per unit canopy area was higher for the parent line (0.2583 mol m^{-2} d^{-1}) compared with line 1 (0.2166 mol m^{-2} d^{-1}) or line 2 (0.2163 mol m^{-2} d^{-1}; see "Materials and Methods").

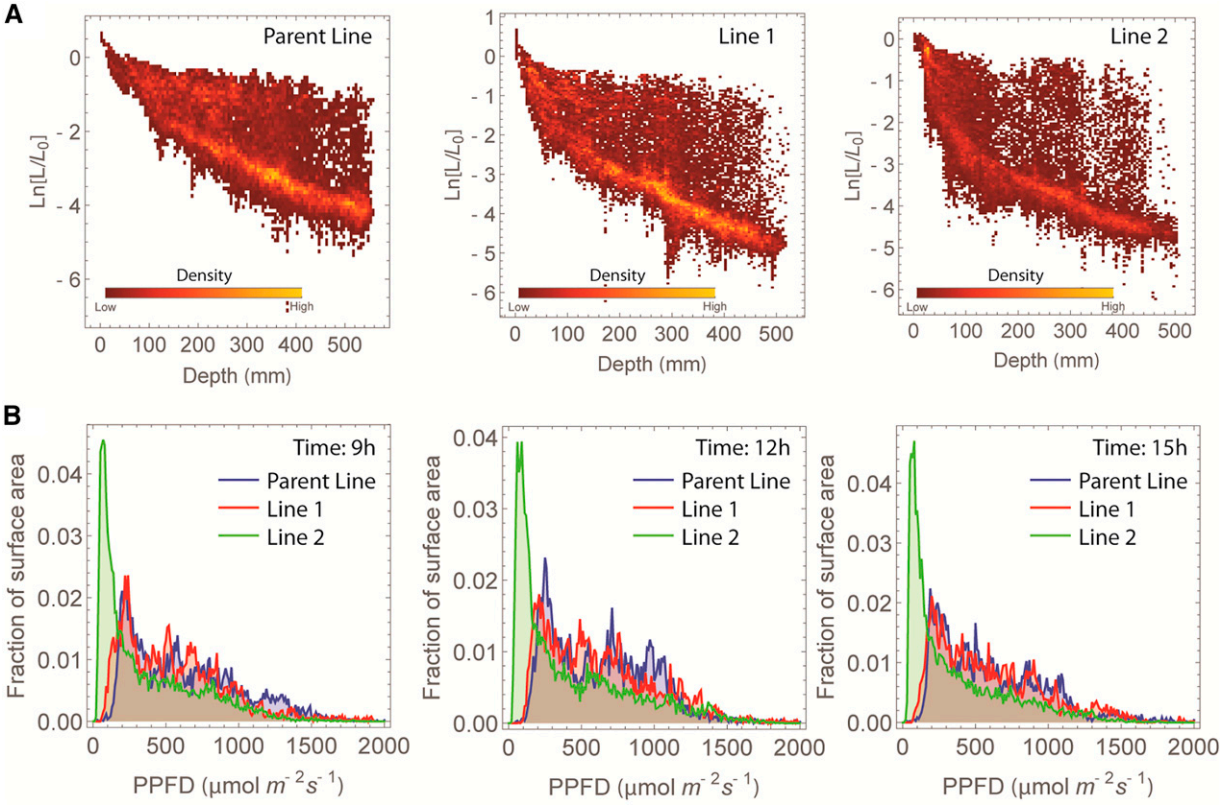

Figure 4. Diagrams depicting the heterogeneity of light environment of the three contrasting wheat canopies. A, Density histogram showing the predicted light levels at 12 PM within each canopy described as the logarithm of the ratio of light received on a horizontal surface to light intercepted by a point on a leaf as a function of depth: parent line (left), line 1 (center), and line 2 (right). B, Frequency of PPFD values according to the fraction of surface area received at the top layer within each canopy: at 9 AM (left), 12 PM, and 3 PM (right).

The probability of photoinhibition diminishes in lower parts of the canopy because of the lower photon flux density, and this is reflected in the F_v/F_m values, with the middle layer (second leaf) approaching the maximal value (0.83; Fig. 7B; Table I). Therefore, the influence of photoinhibition on the top and middle layers only was considered within the model. The strongest photoinhibition (highest reduction in F_v/F_m) was found in the top layer of line 2 followed by line 1 and then, the parent line, whereas the middle layer for all three canopies showed similar F_v/F_m values (Table I). There was a statistically significant difference in F_v/F_m between layers for all lines ($P \leq 0.001$) and no evidence of a significant difference between lines ($P = 0.053$).

The difference between measured F_v/F_m and theoretical maximal F_v/F_m (0.83) was used to calculate a maximal SF according to Equations 6a and 6b (see "Materials and Methods"). Photoinhibition in crops tends show a diurnal pattern from nonexistent at sunrise and sunset to maximal at midday when light levels are in excess. To account for these dynamics, we have fitted parabolas for each layer, with its vertex corresponding to SF_{12} (Supplemental Fig. S2). This SF was used to distort the light response curve as shown in Figure 7. We used the light response curves of CO_2 assimilation for these calculations. It was not possible to use light response curves as a measurement of photoinhibition or quantum yield itself, because a measurement of leaf absorptance would be required.

We applied the SF according to two different scenarios in a manner that describes two contrasting diurnal changes in photoinhibition. In scenario 1, photoinhibition occurs over 6 h over the middle of the day, reaching the maximum value at 12 PM (Supplemental Fig. S4A). In scenario 2, photoinhibition starts at sunrise, peaks in the middle of the day, and decreases until sunset (Supplemental Fig. S4B). Such changes are consistent with those observed across different species, and previous responses for rice (*Oryza sativa*) followed a parabolic-type behavior (Murchie et al., 1999; Demmig-Adams et al., 2012). This approach uses existing knowledge on photoinhibition dynamics under different scenarios as the most effective way of meeting the objectives set out in this study.

The gas exchange and fluorescence parameters used in the model are given in Table I. The values for P_{max} were similar at each level between each of the three

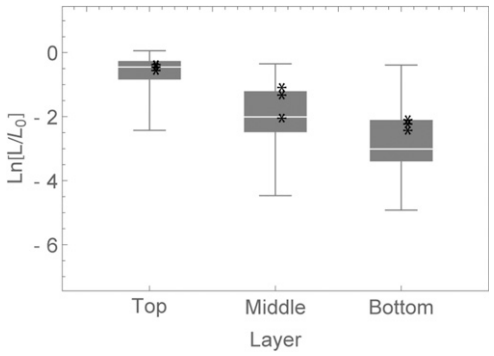

Figure 5. Experimental validation of the predicted light levels. The logarithm of the ratio of light received on a horizontal surface to light intercepted by a point of a leaf ($L_n[L/L_0]$) predicted by ray tracing (box and whiskers) is compared with measurements made manually using a ceptometer (asterisks). Leaves were not all horizontal. Predicted and measured data are for line 2 in top, middle, and bottom layers in the canopy at 12 PM.

plots, with around a 2-fold decrease from upper layer to middle layer and around a 3-fold decrease from middle layer to bottom layer. Because we could not detect photoinhibition in the bottom layer, the F_v/F_m and SF data for layer 3 have been omitted from Table I and thus, will not contribute to the modeled reduction in carbon gain of each of the canopies in this model.

Effect of Photoinhibition on Carbon Gain: Model Output

The mathematical model predicted and compared the simulated daily carbon assimilation under different photoinhibition scenarios as described by Equations 7 to 10 (see "Materials and Methods"). The contribution of the top two layers to a reduction in simulated carbon gain can be seen in Figure 8, A (photoinhibition scenario 1) and B (photoinhibition scenario 2). There is interdependence between distorting both the convexity and the quantum use efficiency values, because light distribution takes a range of values: some of these are more sensitive to the reduction in yield, and some are more sensitive to the reduction in convexity (Long et al., 1994). The strongest effect on net photosynthesis is achieved by a concomitant reduction in both parameters. For scenario 1, reduction in ϕ alone resulted in approximately 1.1%, 2.3%, and 3% reductions in canopy carbon gain in parent line, line 1, and line 2, respectively, and this rose to 2.6%, 4.4%, and 5.6% when combined with θ (Fig. 8A). These represent substantial reductions in potential biomass productivity. These values are increased even further when considering the diurnal dynamics of photoinhibition represented by scenario 2 (Fig. 8B), with reductions in canopy carbon gain rising to 6.8%, 10.2%, and 13.7%, respectively, for a reduction in both ϕ and θ.

The large differences in canopy photosynthesis observed between different lines could result from differences in canopy architecture or differences in susceptibility to photoinhibition on a biochemical level. To investigate, the model was split dependent upon leaf angle within the canopy, which we calculate in a unique way using the triangle surface angle relative to vertical (see "Materials and Methods"; Supplemental Fig. S1A). Rather than a simple measurement of leaf angle subtending the stem and a visual assessment of leaf curvature, this approach allows triangles to form a population derived from every part of the leaf, therefore giving detailed empirical data that can be used against other canopy and physiological data. Results for simulated photoinhibition scenario 1 are shown in Figure 8C, confirming a strong relationship between triangle angle and loss of carbon gain, with line 2 (more visually horizontal leaves) possessing a higher proportion of triangles with higher angles (more horizontal) and suffering more than line 1 or parent lines. This compares well with Figures 3 and 4, which show the upright leaves of lines 1 and 2 with better light penetration and in which a lower proportion of leaf area is photoinhibited (Fig. 7B).

To assess the effects of canopy architecture on the model outputs and determine the predominant drivers, the model was run again on the distribution of PPFD for parent line but this time using the P_{max} and SF values of line 2 and vice versa for comparison. The results can be seen in Figure 8D; positive values indicate a larger percentage reduction in carbon gain in the parent line relative to line 2, whereas negative values indicate a greater reduction in line 2 relative to the parent. The larger percentage reduction when the parent is given the level of photoinhibition shown by line 2 indicates that, although line 2 was probably more susceptible to leaf photoinhibition at least partly as a result of the canopy architecture, the impact of this on a whole-canopy level was in fact minimized by the less vertical leaf structure. The

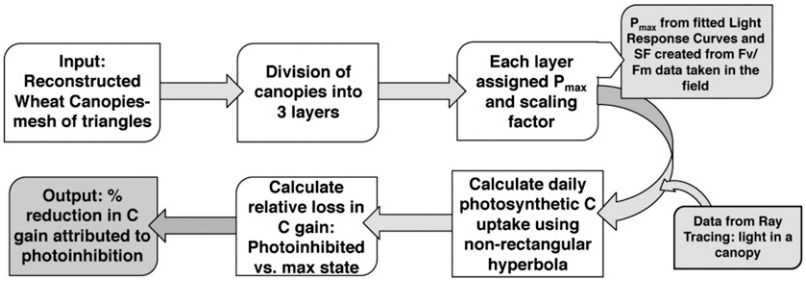

Figure 6. Simplified overview of the modeling method.

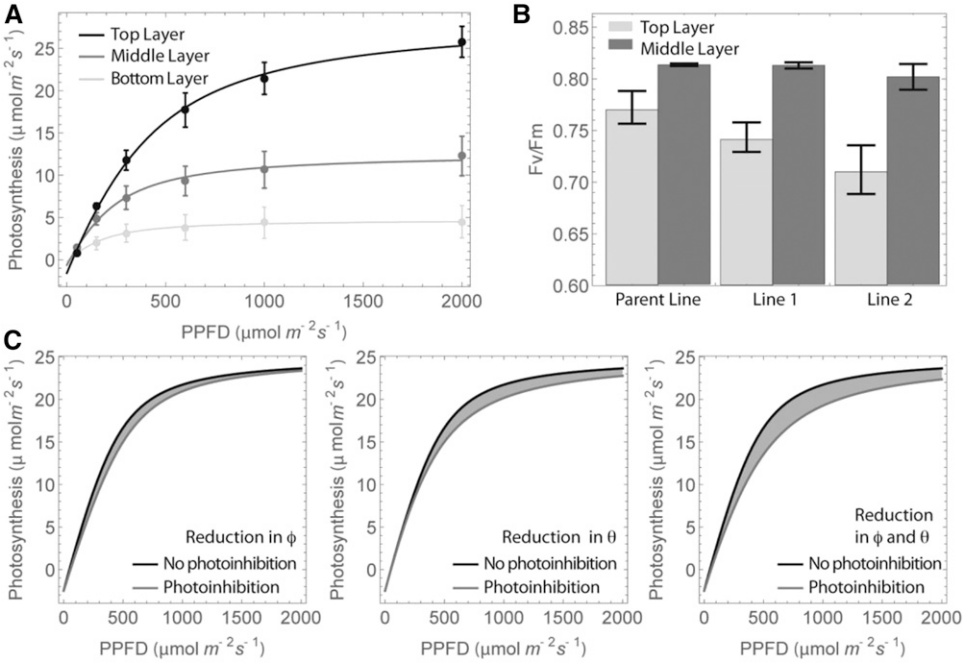

Figure 7. Data used for the parameterization of the photoinhibition model. A, Example light response curves from the top (flag leaf; black), middle (FL-1; dark gray), and bottom (FL-2; light gray) layers of line 2 (light response curves for the parent line and line 1 can be found in Supplemental Fig. S3). Values of the maximum photosynthetic capacity for each layer were obtained from fitting the nonrectangular hyperbola (Eq. 5) to each of the curves. The graph shows the experimental data (mean ± SE of three measurements) and fitted curves. B, Dark-adapted F_v/F_m data per plot and layer measured at 12 PM. The means of five replicates are presented with SEM. C, Distortion of Equation 5 based on parameters from top layer of line 2 and scenario 1 at 12 PM: reduction in ϕ (left), reduction in θ (center), and reduction in ϕ and θ (right).

more open erect structure of the parent is less susceptible to photoinhibition, but in fact, the impact at canopy level will be greater should photoinhibition occur.

Figure 9 combines influence of canopy architecture on the distribution of PPFD (at 12 PM; Fig. 4) with light response curves showing effect of photoinhibition on carbon gain. The strongest effect of photoinhibition is shown, with the largest accumulated distortion between light response curve without and with photoinhibition (gray area in Fig. 9). The average light intensity received by the parent line corresponds to a region of the light response curve that received a greater distortion relative to line 2. It is also positioned higher on the light response curve than line 2. We conclude that the average light-saturated state of a canopy with upright leaves is higher and that the curled nature of leaves at the top of the canopy in line 2 has the effect of oversaturating leaves at the top and overshading at the bottom. The state of light saturation is, therefore, dependent on the relative distribution of leaf area in each layer. This corroborates previous findings and suggests that cLAI will have a strong influence on the tradeoff between photoinhibition susceptibility and impact on long-term canopy carbon gain (Long et al., 2006; Murchie and Reynolds, 2012).

DISCUSSION

High-Resolution Digital Reconstruction of Field-Grown Plants as a Unique Tool

Here, we describe for the first time, to our knowledge, an accurate high-resolution (and rapidly obtained) structural description of canopy geometry from field-grown wheat plants using readily available standard photography techniques (SLR Digital Cameras). This marks a substantial advance from previous work, because we are able to (1) define key structural and photosynthetic features within the canopy and not simply on the upper canopy surface; (2) incorporate features of leaves, such as leaf curvature and twisting; and (3) extract traditional (e.g. extinction coefficient and fractional interception) and unique (e.g. average triangle angle and surface area fraction) canopy measurements that are difficult, if not impossible, to obtain in the field (for example, cLAI, vertical profiling, and leaf tissue angle distributions). These can be extracted directly from the 3D data and not from field measurements using light sensors and geometric measuring tools that are prone to error according to weather and user.

Construction of 3D plants in silico would require knowledge of plant topology and properties, such as leaf and stem length, blade width, tiller number, leaf laminae curvature, or inclination angle. A few models representing 3D canopy architecture for different crops have been developed in recent years; however, these models either simplify the representation of the plants to include only the essential features (Evers et al., 2005) or deduce average architectural parameters from a number of representative plants (Valladares et al., 2005; Song et al., 2013). These methods can be highly time consuming because of the rigorous measurements required (Fourcaud et al., 2008; Vos et al., 2010), and based upon the parameters used, inputting standard leaf angle distributions into a photosynthesis model can lead to a 4% to 15% difference in output compared with models with explicitly described leaf angles (Sarlikioti et al., 2011). Parameterization of functional-structural plant models for wheat was carried out for contrasting densities (Baccar et al., 2011) but not for cultivars with a contrasting architecture.

Table I. *Parameters used in the model*

Layer	F_v/F_m	SF_{12}	P_{max}
Parent line			
Top layer	0.7724 ± 0.01583	0.931	22.3
Middle layer	0.8136 ± 0.00117	0.98	13.6
Bottom layer			4.6
Line 1			
Top layer	0.7436 ± 0.01431	0.896	25.8
Middle layer	0.813 ± 0.00302	0.98	16.9
Bottom layer			6.3
Line 2			
Top layer	0.7122 ± 0.02353	0.857	28.6
Middle layer	0.802 ± 0.01246	0.966	12.6
Bottom layer			4.7
Maximal light response curve values			
Φ			0.052
θ			0.845
α			0.1

Our image-based approach is more likely to capture the heterogeneity of crops within a field, because image-based approaches such as this digitize existing crops, whereas other rule-based methods will create an averaged crop that may capture the general features of the variety/line/species but will not capture unique differences between crops of the same type and thus, may not be as representative or realistic. Furthermore, such rule-based approaches are labor and data intensive and would need to be carried out for each individual line in this case (or species/varieties), whereas this approach may give useable representative canopies within a very short time span.

There was good correspondence between manual and digitized canopy structural measurements, notably the extinction coefficient k. The differences in k seen here are within the range expected for wheat but still show variation that would be expected to result in differences in the relationship between intercepted light and potential productivity (Murchie and Reynolds, 2012). The percentage difference in leaf area between real and reconstructed plants using this method has previously been found to be low (4%; Pound et al., 2014), and a value of 1% was found here (data not shown). The reconstruction method was also able to accurately reproduce similar percentages of stem versus leaf material

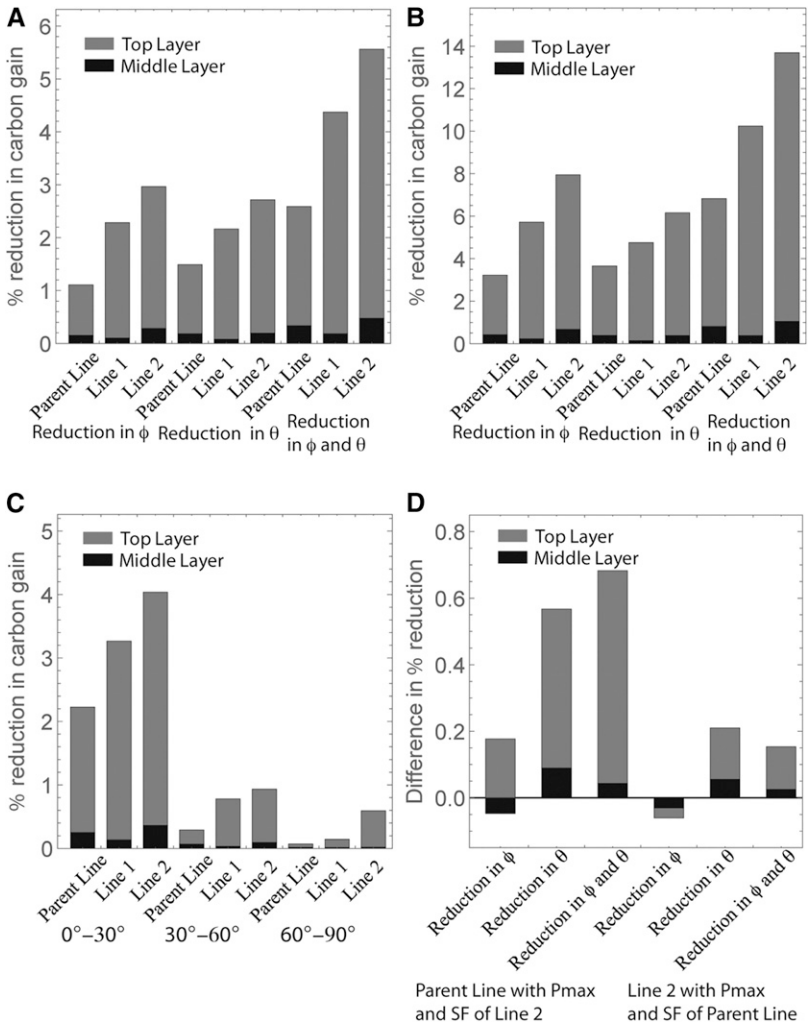

Figure 8. Results of the model: the predicted effect of photoinhibition on carbon gain (Eq. 10). A, Percentage reduction in carbon gain relative to a noninhibited canopy based on photoinhibition scenario 1, with depression in F_v/F_m occurring for 6 h around midday according to a hyperbolic relationship. B, Percentage reduction in carbon gain relative to a nonphotoinhibited canopy based on photoinhibition scenario 2, with depression in F_v/F_m beginning at dawn and ending at dusk according to a hyperbolic relationship. C, Percentage reduction in carbon gain relative to a nonphotoinhibited canopy based photoinhibition on scenario 1 as a function of the triangle angle relative to vertical. Results are for a distortion in both ϕ and θ. D, Graph indicating the importance of canopy architecture on the model output. The P_{max} and SF according to photoinhibition scenario 1 of line 2 were applied to the canopy and ray-tracing output of the parent line and vice versa. The difference in the percentage reduction in carbon gain was then calculated relative to the results obtained from the donor line. Positive values indicate a greater reduction in carbon gain for the parent line, whereas negative values indicate a greater reduction for line 2.

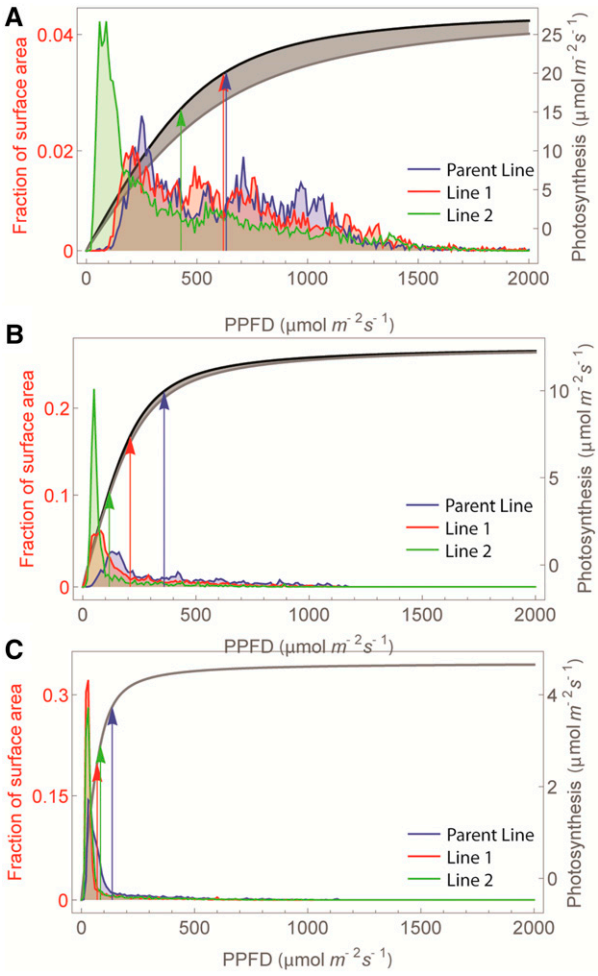

Figure 9. Graph indicating the frequency of light levels as a function of the fraction of the total surface area of the canopy received at 12 PM by the top (A), middle (B), and bottom (C) layers in each canopy and the average irradiance, indicated by arrows, overlaid on the light response curve and distorted light response curve of line 2.

(around 30% stem content by area for each of the three lines).

The predicted light distribution taken from ray-tracing data shows the spatial and temporal heterogeneity within all three wheat canopies resulting from their differences in architecture. Achieving such high resolution with measurements in the canopy would not be possible, and any attempt would require vast amounts of sensors and data processing. This tool could provide a low-cost but detailed method for phenotyping for both small-scale and advanced systems.

Accounting for Carbon Loss at the Whole-Canopy Level

We have used the highly accurate digitized 3D reconstructions to scale up photosynthetic processes to the whole-canopy level. Because the ray-tracing parameters day and latitude were kept the same and all gas exchange and fluorescence measurements were taken within the same period, any observed differences in photosynthetic activity were associated with genetically determined differences (e.g. plant architecture) and not with diurnal solar movement.

Susceptibility to photoinhibition and its dynamics is dependent on species, cultivar, and conditions, and thus, changes in F_v/F_m are not fixed (Murchie et al., 1999; Demao and Xia, 2001; Demmig-Adams et al., 2012). Values of photosynthetic capacity and the dark-adapted fluorescence parameters were used for model parameterization. Previous models used a photon dose effect to predict levels of photoinhibition (Werner et al., 2001; Zhu et al., 2004). We did not adopt this approach, because we wished to avoid potential genotype-specific differences in required dosage. We chose instead to use field measurements of F_v/F_m to predict photoinhibition at different canopy positions and times of day (Leverenz, 1994), because F_v/F_m is an actual measure of PSII quantum yield (Murchie and Lawson, 2013). To present a realistic picture of the potential for the impact of photoinhibition on canopy photosynthesis, variation in the dynamics of photoinhibition was explored in two different scenarios (results in Fig. 8, A and B; dynamics in Supplemental Fig. S4). In the first scenario, we restricted simulated photoinhibition to the hours surrounding midday (commonly seen for fast-growing plants, such as cereals; Murchie et al., 1999), and in the second scenario, we assumed that it would start from the hours after dawn, which is more commonly seen in slower-growing stress-tolerant plants. When the dynamics are altered to represent depression in F_v/F_m over the whole day (scenario 2), the percentage reduction in carbon gain is much greater (Fig. 8B). These results indicate the flexibility of this modeling technique and highlight the impact of precise architecture for different photoinhibition dynamics.

Using measured photoinhibition data in the field, we have found up to a 5.6% (scenario 1) or 13.7% (scenario 2) reduction in carbon gain solely because of photoinhibition with the parent line exhibiting the smallest amount of carbon loss (line 2 had the greatest amount, and line 1 had an intermediate amount). This loss is largely caused by the measured differences in F_v/F_m and thus, the resultant SF between lines in the uppermost layer. The parent line has a more upright, straight-leaved phenotype, whereas line 2 exhibits a greater amount of leaf curling, particularly in the top layer, with line 1 exhibiting an intermediate phenotype. It is highly likely that this was a result of the canopy architecture and not inherent genetic differences in photoinhibition susceptibility between the lines, which are shown by Figure 8D. It is established that the leaf angle in relation to solar position is a strong determinant of radiation and heat load (He et al., 1996; Murchie et al., 1999).

The higher potential productivity of canopies with vertical leaves has been well documented and is largely because of a combination of higher optimal

cLAI and a lowered overall state of photosynthetic saturation of the crop canopy (Murchie and Reynolds, 2012; Song et al., 2013). Our data provide a more sophisticated analysis of real in-canopy light distribution, and we conclude that the state of light saturation of the upright canopy (parent line) was actually higher than that of the closed canopy (line 2). The proportion of leaves in a severely light-limited state is, therefore, of critical importance (Murchie et al., 2002; Long et al., 2006). Figure 8 shows that the parent line is closer to saturation at the top and middle layers (compared with line 2), has a higher canopy photosynthesis, and also, has spare capacity for increasing the overall canopy photosynthetic rate in all layers regardless of photoinhibition.

It is important to calculate percentage carbon loss caused by lowered quantum yield. Our three contrasting wheat canopies have inherent differences in potential canopy photosynthesis (shown above). The values observed are generally in line with a numerical study based on artificially constructed canopies that observed a decline of daily photosynthesis of 6% to 8% (Werner et al., 2001). Zhu et al. (2004) found a 12% to 30% decrease of daily integral carbon uptake because of thermal dissipation of absorbed light energy with the largest reduction from a top layer.

Managing and Mitigating Photoinhibition

Here, we extend earlier work on the impact of photoinhibition at the canopy scale, and we reveal how canopy structure, photosynthesis, and photoinhibitory loss are intimately connected within unique highly accurate 3D reconstructions of field-grown plants. We use the light-induced lowering of quantum yield in optimal conditions where there is no other stress factor present that may preinduce a lowered F_v/F_m value. Accumulation of carbohydrate has been suggested in some species to precede photoinhibition. However, this is highly unlikely in fast-growing unstressed cereals where diurnal patterns of leaf carbohydrate do not follow patterns of photoinhibition (Murchie et al., 2002; Demmig-Adams et al., 2012). In terms of productivity, the best strategy is of course to minimize photoinhibition in all circumstances at the biochemical level. Photoprotective mechanisms, such as the xanthophyll cycle and PsbS-dependent quenching, are known to reduce the level of photoinhibition in leaves (Li et al., 2002; Niyogi et al., 2005). It has been pointed out that such approaches may need to consider costs as well as benefits of high levels of thylakoid-level photoprotection (Hubbart et al., 2012). If this is the case, then the role of canopy architecture in this tradeoff needs to be carefully considered.

We can discern strategies for dealing with the effects of photoinhibition at this level: restrict substantial levels of photoinhibition to the top layers by closing the canopy to protect the lower layers and ensure a high degree of saturation of the upper layers or attempt a higher overall productivity with a vertical structure but risk a greater impact on canopy carbon gain should photoinhibition occur. The former will result in a canopy with an inherently lower productivity that is still susceptible to localized photoinhibition in upper layers. Previously, it has been shown clearly that upright leaves have a lower susceptibility to photoinhibition (Murchie et al., 1999), and this would seem to be synergistic with the higher inherent productivity of such architecture. However, our data suggest that the tolerance conferred by leaf posture is not sufficient to avoid loss completely and that upright canopies should be selected to have a high tolerance to photoinhibition on a leaf level.

The importance of photoinhibition may come down to the level of sunshine hours that a crop canopy experiences during key yield-forming stages. For this study, we used sunny days to measure F_v/F_m, and we calculate that such days were restricted to less than 30 d of the total for the postanthesis period. Photoinhibition will be strongest in crops grown in high-yield potential, high-radiation environments, and these would see the greatest loss in yield as a result of photoinhibition alone. This will be true for many irrigated rice and yield environments. In the case of tropical rice, there is known genotypic diversity in susceptibility (Murchie et al., 1999; Demao and Xia, 2001) that may be the result of genetically determined nonphotochemical quenching levels (Kasajima et al., 2011). It is highly probable that we can improve biomass and yield by optimizing photoinhibition, and this requires understanding of the existing canopy architecture. The next step is to isolate genetic variation in photoprotection (e.g. resulting from PsbS expression) by incorporating the effect of canopy position.

CONCLUSION

In this study, we used an empirical model to investigate the interactions between plant architecture and solar irradiance. Unique highly realistic digital reconstruction combined with simulation of light intercepted by leaves and prediction of carbon assimilation represent a unique method to investigate complex plant-environment interactions and provide a method of scaling up to the whole-canopy level and exploring the importance of canopy architecture.

Plant phenotyping is an important tool in screening crops for future breeding. As we show in this study, image-based 3D plant reconstruction was successfully applied to test how plant architecture influences photosynthesis and photoinhibition. The extracted features (cLAI, vertical profile, and angle distribution) showed clear differences between three contrasting wheat lines. In a similar way, all wheat lines showed differences in canopy light distribution. We found that larger carbon losses were associated with a higher light extinction coefficient. Whole-canopy carbon gain can be protected (under photoinhibition) if spatial distribution of light in the lower canopy is improved.

MATERIALS AND METHODS

Plant Material

Wheat (*Triticum aestivum*) lines with contrasting canopy architectures were selected from an ongoing field trial at the University of Nottingham farm; 138 double-haploid lines were developed jointly by Nottingham and the International Maize and Wheat Improvement Centre from a cross between the International Maize and Wheat Improvement Centre large-ear phenotype spring wheat advanced line LSP2 and the United Kingdom winter wheat 'Rialto.' Back crossed 3 (BC3) lines were generated from three backcrosses between selected double-haploid lines as donors and a spring elite cultivar (cv Ashby) or a winter cultivar (cv Humber) as recipient. The BC3 lines were then self-fertilized for five generations to produce BC3S5 lines used in this experiment. This approach resulted in the formation of a large number of stable lines with contrasting canopy architecture but photosynthetic responses consistent with the United Kingdom environment (Driever et al., 2014). Three wheat lines were selected for analysis: cv Ashby (parent line), cv 32-129bc (line 1), and cv 23-74bc (line 2).

A field experiment was carried out at Sutton Bonington (52° 83′ N, 1° 25′ W) in 2013 and 2014 on BC3S5 lines and the recurrent parents cv Ashby and cv Humber. The soil was a medium sandy loam 0.8-m deep over clay (Dunington Heath Series). The experiment used a randomized block design with two replicates, and the plot size was 1.65 × 6 m; there were 12 rows with a row width of 13.2 cm. The previous crop was oilseed rape (*Brassica napus*). The plots were sown on November 18, 2013 at a seed rate of 300 seeds m^{-2}. In each plot, 220 kg N ha^{-1} nitrogenous fertilizer as ammonium nitrate was applied in a three-split program; 40 kg N ha^{-1} was applied in early March, 100 kg N ha^{-1} was applied in late March, and 80 kg N ha^{-1} was applied in early May. Plant growth regulator chlormequat was applied at growth stage 31 (stem elongation and first node detectable). Prophylactic applications of fungicides were given at growth stages 31, 39, and 59 (Tottman, 1987) to keep diseases to very low levels. Pesticides and herbicides were used as necessary to minimize the effects of pests and weeds.

Imaging and Ray Tracing

3D analysis of plants was made according to the protocol by Pound et al. (2014). The developmental stage of each of the lines was the same. At anthesis and after photosynthesis measurements, wheat plants (roots and shoots) were carefully removed from the field, taken to a laboratory, and packed in a box to avoid excessive movement or damage to leaves. Roots were supplied with water to prevent wilting. It was found that this process did not alter the key architectural features of the plants. They were imaged within 2 h using three fixed Canon 650D cameras, with a minimum of 40 images per plant. Images were captured using a revolving turntable, including a calibration target of set width (397 mm) that was used to both aid with automatic camera calibration and enable scaling of the model to the correct size after reconstruction. An initial point cloud was obtained using the PMVS software (Furukawa and Ponce, 2010; Wu, 2011). The PMVS photometric consistency threshold (Furukawa and Ponce, 2010; Eq. 2) was set at 0.45 to optimize the amount of plant material recognized in the point cloud. Default parameters were used within the Reconstructor software, except for maximum cluster size and boundary sample rate, which were changed to 120 and 15, respectively. These parameters were chosen, because they reduce the number of triangles in the output mesh but give the most accurate mesh (in terms of both total area and Hausdorff distance) in optimization tests (data not shown).

Three replicate plants representative of the morphology of each line were taken from each line and reconstructed; however, for lines 1 and 2, two plants were used to form the final canopy. The wheat ears were manually removed from the resultant mesh, because the reconstructing method is unable to accurately represent their form. Canopies were created for each of the three plots by duplicating and randomly rotating the reconstructions in a 3 × 3-grid pattern. The orientations were altered until the cLAI of the plot matched the average value given from leaf and stem area measurements of the sampled plants (Supplemental Table S2). Reconstructed canopies consist of n triangles with coordinates of the ith triangle given by a vector $\{x_i^1, y_i^1, z_i^1, x_i^2, y_i^2, z_i^2, x_i^3, y_i^3, z_i^3\}$, where coordinates x and y correspond to the coordinates on the ground and coordinate z corresponds to height above the ground.

Total light per unit leaf area for the ith triangle at time t, $L_i(t)$, was predicted using a forward ray-tracing algorithm implemented in fastTracer (fastTracer, version 3; PICB; Song et al., 2013). Latitude was set at 53 (for Sutton Bonington, United Kingdom), atmospheric transmittance was 0.5, light reflectance was 7.5%, light transmittance was 7.5%, and day was 181 (June 30), with sunrise and sunset of 5 AM and 10 PM, respectively. The diurnal course of light intensities over a whole canopy was recorded in 1-h intervals. To prevent the boundary effect, we positioned the ray-tracing boundaries at centers of the outer plants. The software fires rays through a box with defined boundaries; when they exit one boundary (i.e. the side), they enter again from the opposite side.

Leaf Angle, Dry Weight, and Leaf Area Measurements

Leaf angles were measured in two different ways. Leaf angles were measured in the field using a protractor (Pask et al., 2012), with the average of five measurements per layer per line. These values were then compared with those obtained on the reconstructed plants using a mesh editing software (Meshlab. sourceforge.net; Supplemental Table S1). Plant dry weight and area were analyzed by separating shoot material into steam, flag leaf, and all other leaves before passing them through a leaf area meter (LI3000C; Licor) followed by drying each component individually in an oven at 80°C for 2 d until no more weight loss was noted. Plants were weighed immediately. Leaf and stem areas were also calculated for the reconstructions using Meshlab for comparison.

Field Data: Gas Exchange and Fluorescence

Data were taken from the field-grown wheat in plots in the same week in which the imaged plants were taken on Sutton Bonington Campus. Leaf gas exchange measurements were taken with a Licor 6400XT IR Gas-Exchange Analyzer (Licor). The block temperature was maintained at 20°C using a flow rate of 500 mL min^{-1}. Light was provided by a combination of in-built red and blue light-emitting diodes. Light response curves were taken on leaves that had not been dark adapted. Illumination occurred over a series of six photosynthetically active radiation values between 50 and 2,000 μmol m^{-2} s^{-1}, with a minimum of 2 min at each light level. Light response curves were taken at three different canopy heights: labeled top, middle, and bottom referring to flag leaf, second leaf (Flag leaf −1 [FL −1]), and third leaf (FL −2), respectively, with height above ground being noted. Leaves in the middle and bottom layers were additionally exposed to a photosynthetically active radiation level of 500 μmol m^{-2} s^{-1} for 3 min before the light response curve measurements. Four replicates were taken per plot for each canopy layer.

A Walz (Effeltrich) MiniPam Fluorometer was used to measure dark-adapted values of F_v/F_m in the field wheat at midday. Leaves were dark adapted using clips (DLC-08; Walz) for 20 min, and initial (minimum) PSII fluorescence in the dark-adapted state and F_m were measured by applying a saturating pulse (0.8 s at 6,000 μmol m^{-2} s^{-1}). Four replicates were taken per plot per layer, but as values for the middle layer were approaching or at the maximal value expected ($F_v/F_{m\,max}$ = 0.83), measurements were not taken for the bottom layer.

cLAI and the Light Extinction Coefficient

cLAI (leaf area per unit ground area as a function of depth) was calculated from each of the canopy reconstructions. For each depth (d; distance from the highest point of the canopy), we found all triangles with centers lying above d (Eq. 1):

$$d_i = \max_{j=1,2,3;1\le i\le n} z_i^j - \left(z_i^1 + z_i^2 + z_i^3\right)/3 \quad (1)$$

We then calculated the sum of the areas of these triangles and divided this sum by ground area. The cLAI as a function of depth through the canopy was calculated using Equation 2:

$$\mathrm{cLAI}(d) = \frac{\sum_{i=1}^{n} I(d_i \le d) S_i}{\left(\max_{1\le i\le n} x_i - \min_{1\le i\le n} x_i\right)\left(\max_{1\le i\le n} y_i - \min_{1\le i\le n} y_i\right)} \quad (2)$$

where $I(A) = 1$ if condition A is satisfied, and S_i is the area of a triangle i.

The light extinction coefficient of the canopy was calculated using the 3D structural data and the light distribution obtained from ray tracing. To calculate fractional interception within a canopy as a function of depth at time t, we first identified all triangles above depth d (Eq. 1). We then calculated their contribution to intercepted light by multiplying PPFD received per unit surface area (ray-tracing output) by the area of triangle. The light intercepted was summed for all triangles above the set d, and we divided by light intercepted by ground area according to Equation 3:

$$F(d,t)=\frac{\sum_{i=1}^{n} I(d_i \le d)\ S_i L_i(t)}{L_0(t)\times \text{ground area}} \quad (3)$$

where $L_0(t)$ is light received on a horizontal surface with a ground area $(\max_{1\le i\le n}x_i-\min_{1\le i\le n}x_i)(\max_{1\le i\le n}y_i-\min_{1\le i\le n}y_i)$, and $L_i(t)$ is light intercepted by a triangle i.

The light extinction coefficient, k, was calculated by fitting (by least squares) the function

$$f(x)=a\left(1-e^{-kx}\right) \quad (4)$$

to the set of points {cLAI(d), $F(d,t)$} calculated by varying depth from 0 to the height at total cLAI with step Δd = 1 mm (Supplemental Fig. S4); a in Equation 4 is a fitted parameter.

Model Setup

A simplified overview of the modeling process is given in Figure 6.

All modeling was carried out using Mathematica (Wolfram). The response of photosynthesis to light irradiance, L, was calculated using a nonrectangular hyperbola given by Equation 5:

$$F_{NRH}(L,\phi,\theta,P_{max},\alpha)=\frac{\phi\ L+(1+\alpha)P_{max}-\sqrt{(\phi L+(1+\alpha)P_{max})^2-4\theta\phi L(1+\alpha)P_{max}}}{2\theta}-\alpha P_{max} \quad (5)$$

The nonrectangular hyperbola is defined by four parameters: the quantum use efficiency ϕ, the convexity θ, the maximum photosynthetic capacity P_{max}, and the rate of dark respiration R_d. We assumed that the rate of dark respiration is proportional to the maximum photosynthetic capacity according to the relationship $R_d=\alpha P_{max}$ (Givnish, 1998; Niinemets and Tenhunen, 2007; Retkute et al., 2015), where α = 0.1.

Values for P_{max} were determined from leaf gas exchange measurements ("Field Data: Gas Exchange and Fluorescence"). Curve fitting was carried out using the Mathematica command FindFit with a minimum constraint on dark respiration at 0.05 and convexity at 0.6. Data and fitted curves are shown in Figure 7A (line 2) and Supplemental Figure S3 (parent line and line 1). Estimated values of P_{max} for each layer and each canopy are given in Table I. The gas exchange measurements and resulting fitted light response curves were not sufficient to determine convexity and absolute values of quantum yield, because (1) we did not have a measurement of leaf absorptance and (2) we could not be certain of the state of photoinhibition of the leaf during the gas exchange measurements because of the protocol used. Hence, the model distorts the light response curve from a known uninhibited state using the F_v/F_m data to set the change in quantum yield. As described above, there is a variable dependence of convexity on quantum yield (Long et al., 1994). We set maximal value for quantum use efficiency at 0.052 and convexity at 0.845 (Table I; Leverenz 1994; Werner et al., 2001).

To account for photoinhibition, we assumed that the quantum use efficiency and convexity change during the course of a day (Fig. 7C; i.e. each or both are reduced according to the SF, which is parameterized using F_v/F_m measurements taken in the field; Genty et al., 1989; Leverenz, 1994). The maximum photoinhibition was assumed to be present at 12 PM ("Field Data: Gas Exchange and Fluorescence"), giving the SF

$$SF_{12}=\frac{(F_v/F_m)}{(F_v/F_{m_{max}})} \quad (6a)$$

Two different scenarios of diurnal changes in photoinhibition were modeled to represent different responses to photoinhibition (Demmig-Adams et al., 2012). Scenario 1 showed a depression in F_v/F_m over the 6 h around midday, which may be more appropriate for herbaceous fast-growing plants, such as cereals (Murchie et al., 1999), whereas scenario 2 showed a depression in F_v/F_m starting at sunrise, peaking in the middle of the day, and ending at sunset. To represent these dynamics, we fitted a parabola (Eq. 6b) using the least squares method through points {t_0,1}, {12,SF_{12}}, and {t_N,1}, where t_0 and t_N indicate the onset and ending of the photoinhibition period (t_0 = 9 AM and t_N = 3 PM for photoinhibition scenario 1 and t_0 = 5 AM and t_N = 10 PM for photoinhibition scenario 2), respectively:

$$SF(t)=at^2+bt+c \quad (6b)$$

The dynamics of each of the photoinhibition scenarios for each canopy are given in Supplemental Fig. S5.

The carbon assimilation at triangle i was calculated by combining Equation 5 with the predicted PPFD at triangle I for each hour. Daily carbon assimilation, P_i (Eq. 7), was then calculated by integrating the rate of photosynthetic carbon uptake over the day (from 5 AM to 10 PM) and multiplying by the area of the triangle, S_i:

$$P_i=S_i\int_5^{22} F_{NRH}(L_i(t),\phi,\theta,P_{max},\alpha)dt \quad (7)$$

The daily carbon assimilation under photoinhibition, P_i^{PIH}, was calculated by scaling the appropriate parameters in Equation 5 according to an SF value at time t (Eqs. 8a–8c), namely (1) reduction in quantum use efficiency (only ϕ multiplied by the SF):

$$P_i^{PIH}=S_i\int_5^{22} F_{NRH}(L_i(t),SF(t)\times\phi,\theta,P_{max},\alpha)dt \quad (8a)$$

(2) reduction in convexity (only θ multiplied by the SF):

$$P_i^{PIH}=S_i\int_5^{22} F_{NRH}(L_i(t),\phi,SF(t)\times\theta,P_{max},\alpha)dt \quad (8b)$$

and (3) reduction in quantum use efficiency and convexity (both θ and ϕ multiplied by the SF):

$$P_i^{PIH}=S_i\int_5^{22} F_{NRH}(L_i(t),SF(t)\times\phi,SF(t)\times\theta,P_{max},\alpha)dt \quad (8c)$$

Because each canopy was divided into three layers, each triangle from the digital plant reconstruction was assigned to a particular layer m according to the triangle center (i.e. with triangle center between upper and lower limits of a layer depth). Carbon gain per unit canopy area was calculated as daily carbon assimilation over a whole canopy divided by the total surface area of the canopy according to Equation 9:

$$C=\frac{\sum_{i=1}^{n}P_i}{\sum_{i=1}^{n}S_i} \quad (9)$$

The reduction in carbon gain because of the photoinhibition for layer m (where m = 1 or 2; referring to the top and middle layers, respectively) was calculated as the percentage difference between daily carbon gain without photoinhibition (using the unscaled light response curve) and with photoinhibition (scaled light response curve) summed over all of the triangles belonging to the layer m according to Equation 10:

$$\Delta C_m=100\frac{\sum_{i=1}^{n} I\left(d_m^L\le d_i<d_m^U\right)\left(P_i-P_i^{PIH}\right)}{\sum_{i=1}^{n}P_i} \quad (10)$$

Where P_i is calculated using Equation 7, and P_i^{PIH} is calculated using Equations 8a to 8c.

The reduction in whole-plant daily carbon gain because of photoinhibition is obtained as a sum over the top two layers:

$$\Delta C=\Delta C_1+\Delta C_2 \quad (11)$$

Supplemental Data

The following supplemental materials are available.

Supplemental Figure S1. Leaf angle frequency.

Supplemental Figure S2. PPFD distribution within canopy at different times of the day.

Supplemental Figure S3. Measured light response curves at different canopy positions.

Supplemental Figure S4. Cumulative leaf area index against fractional interception.

Supplemental Figure S5. Scaling factors used for different scenarios of photoinhibition.

Supplemental Table S1. Leaf angle for measured versus reconstructed canopies.

Supplemental Table S2. Reconstruction and canopy details.

Supplemental Table S3. Symbol definitions.

ACKNOWLEDGMENTS

We thank Dr. Xinguang Zhu and Dr. Qinfeng Song (Shanghai Institute for Biological Sciences, Chinese Academy of Sciences) for useful discussion regarding the Fast Trace Program; Dr. Ian Smillie (ADAS UK Ltd), Kannan Chinnathambi, and Jamie Randall (University of Nottingham) for field measurements; Christiane Werner (University of Bayreuth) for useful discussion of photoinhibition modeling at the outset of this work; and Dr. Peter Werner and Dr. Jacob Lage (KWS UK Ltd) for development of the BC3 wheat lines and permission to use them in this study.

Received May 17, 2015; accepted August 14, 2015; published August 17, 2015.

LITERATURE CITED

Baccar R, Fournier C, Dornbusch T, Andrieu B, Gouache D, Robert C (2011) Modelling the effect of wheat canopy architecture as affected by sowing density on Septoria tritici epidemics using a coupled epidemic-virtual plant model. Ann Bot (Lond) **108:** 1179–1194

Björkman O, Demmig B (1987) Photon yield of O2 evolution and chlorophyll fluorescence characteristics at 77 K among vascular plants of diverse origins. Planta **170:** 489–504

Demao J, Xia L (2001) Cultivar differences in photosynthetic tolerance to photooxidation and shading in rice (Oryza sativa L.). Photosynthetica **39:** 167–175

Demmig-Adams B, Cohu CM, Muller O, Adams WW III (2012) Modulation of photosynthetic energy conversion efficiency in nature: from seconds to seasons. Photosynth Res **113:** 75–88

Driever SM, Lawson T, Andralojc PJ, Raines CA, Parry MAJ (2014) Natural variation in photosynthetic capacity, growth, and yield in 64 field-grown wheat genotypes. J Exp Bot **65:** 4959–4973

Evans JR, Jakobsen I, Ogren E (1993) Photosynthetic light-response curves: 2. Gradients of light-absorption and photosynthetic capacity. Planta **189:** 191–200

Evers JB, Vos J, Fournier C, Andrieu B, Chelle M, Struik PC (2005) Towards a generic architectural model of tillering in Gramineae, as exemplified by spring wheat (Triticum aestivum). New Phytol **166:** 801–812

Fourcaud T, Zhang X, Stokes A, Lambers H, Körner C (2008) Plant growth modelling and applications: the increasing importance of plant architecture in growth models. Ann Bot (Lond) **101:** 1053–1063

Furukawa Y, Ponce J (2010) Accurate, dense, and robust multiview stereopsis. IEEE Trans Pattern Anal Mach Intell **32:** 1362–1376

Genty B, Briantais JM, Baker NR (1989) The relationship between the quantum yield of photosynthetic electron transport and quenching of chlorophyll fluorescence. Biochim Biophys Acta **990:** 87–92

Givnish TJ (1988) Adaptation to sun and shade: a whole-plant perspective. Aust J Plant Physiol **15:** 63–92

He J, Chee C, Goh C (1996) "Photoinhibition" of Heliconia under natural tropical conditions: the importance of leaf orientation for light interception and leaf temperature. Plant Cell Environ **19:** 1238–1248

Hirose T (2005) Development of the Monsi-Saeki theory on canopy structure and function. Ann Bot **9:** 483–494

Hubbart S, Ajigboye OO, Horton P, Murchie EH (2012) The photoprotective protein PsbS exerts control over CO(2) assimilation rate in fluctuating light in rice. Plant J **71:** 402–412

Kasajima I, Ebana K, Yamamoto T, Takahara K, Yano M, Kawai-Yamada M, Uchimiya H (2011) Molecular distinction in genetic regulation of nonphotochemical quenching in rice. Proc Natl Acad Sci USA **108:** 13835–13840

Krause GH, Weis E (1991) Chlorophyll fluorescence and photosynthesis: the basics. Annu Rev Plant Physiol Plant Mol Biol **42:** 313–349

Leverenz JW (1994) Factors determining the nature of the light dosage response curves of leaves. *In* NR Baker, JR Bowyer, eds, Photoinhibition of Photosynthesis: From Molecular Mechanisms to the Field. Bios Scientific Publishing, Oxford, pp 239–254

Li XP, Muller-Moule P, Gilmore AM, Niyogi KK (2002) PsbS-dependent enhancement of feedback de-excitation protects photosystem II from photoinhibition. Proc Natl Acad Sci USA **99:** 15222–15227

Long SP, Hällgren JE (1985) Measurement of CO_2 assimilation by plants in the field and in the laboratory. *In* J Coombs, DO Hall, SP Long, JMO Scurlock, eds, Techniques in Bioproductivity and Photosynthesis. Pergamon Press, Oxford, pp 62–94

Long SP, Humphries S, Falkowski PG (1994) Photoinhibition of photosynthesis in nature. Annu Rev Plant Physiol Plant Mol Biol **45:** 633–662

Long SP, Zhu XG, Naidu SL, Ort DR (2006) Can improvement in photosynthesis increase crop yields? Plant Cell Environ **29:** 315–330

Murchie EH, Chen Yz, Hubbart S, Peng S, Horton P (1999) Interactions between senescence and leaf orientation determine in situ patterns of photosynthesis and photoinhibition in field-grown rice. Plant Physiol **119:** 553–564

Murchie EH, Hubbart S, Chen Y, Peng S, Horton P (2002) Acclimation of rice photosynthesis to irradiance under field conditions. Plant Physiol **130:** 1999–2010

Murchie EH, Lawson T (2013) Chlorophyll fluorescence analysis: a guide to good practice and understanding some new applications. J Exp Bot **64:** 3983–3998

Murchie EH, Reynolds MP (2012) Crop radiation capture and use efficiency. *In* RA Meyers, Encyclopedia of Sustainability Science and Technology. Springer, New York, pp 2615–2638

Niinemets U, Tenhunen JD (1997) A model separating leaf structural and physiological effects on carbon gain along light gradients for the shade-tolerant species Acer saccharum. Plant Cell Environ **20:** 845–866

Niyogi KK, Li XP, Rosenberg V, Jung HS (2005) Is PsbS the site of non-photochemical quenching in photosynthesis? J Exp Bot **56:** 375–382

Ögren E, Sjöström M (1990) Estimation of the effect of photoinhibition on the carbon gain in leaves of a willow canopy. Planta **181:** 560–567

Ort DR, Baker NR (1988) Consideration of the photosynthetic efficiency at low light as a major determinant of crop photosynthetic performance. Plant Physiol Biochem **26:** 555–565

Pask AJD, Pietragalla J, Mullan, Reynolds MP (2012) Physiological Breeding. II. A Field Guide to Wheat Phenotyping. International Wheat and Maize Improvement Centre (CIMMYT), Mexico City, Mexico

Pearcy RW (1990) Sunflecks and photosynthesis in plant canopies. Annu Rev Plant Physiol Plant Mol Biol **41:** 421–453

Pound MP, French AP, Murchie EH, Pridmore TP (2014) Automated recovery of three-dimensional models of plant shoots from multiple color images. Plant Physiol **166:** 1688–1698

Powles SB (1984) Photoinhibition of photosynthesis induced by visible light. Ann Rev Plant Physiol Plant Mol Biol **35:** 15–44

Raven JA (2011) The cost of photoinhibition. Physiol Plant **142:** 87–104

Retkute R, Smith-Unna SE, Smith RW, Burgess AJ, Jensen OE, Johnson GN, Preston SP, Murchie EH (2015) Exploiting heterogeneous environments: does photosynthetic acclimation optimize carbon gain in fluctuating light? J Exp Bot **66:** 2437–2447

Russell G, Jarvis PG, Monteith J (1989) Absorption of radiation by canopies and stand growth. *In* G Russell, B Marshall, P Jarvis, eds, Plant Canopies: Their Growth, Form and Function. Cambridge University Press, Cambridge, United Kingdom, pp 21–41

Sarlikioti V, de Visser PHB, Marcelis LFM (2011) Exploring the spatial distribution of light interception and photosynthesis of canopies by means of a functional-structural plant model. Ann Bot (Lond) **107:** 875–883

Song Q, Zhang G, Zhu XG (2013) Optimal crop canopy architecture to maximise canopy photosynthetic CO2 uptake under elevated CO2: a theoretical study using a mechanistic model of canopy photosynthesis. Funct Plant Biol **40:** 109–124

Takahashi S, Badger MR (2011) Photoprotection in plants: a new light on photosystem II damage. Trends Plant Sci **16:** 53–60

Terashima I, Saeki T (1985) A new model for leaf photosynthesis incorporating the gradients of light environment and of photosynthetic properties of chloroplasts within a leaf. Ann Bot **56:** 489–499

Tottman DR (1987) The decimal code for the growth stages of cereals, with illustrations. Ann Appl Biol **110:** 441–454

Valladares F, Dobarro I, Sánchez-Gómez D, Pearcy RW (2005) Photoinhibition and drought in Mediterranean woody saplings: scaling effects and interactions in sun and shade phenotypes. J Exp Bot **56:** 483–494

Vos J, Evers JB, Buck-Sorlin GH, Andrieu B, Chelle M, de Visser PHB (2010) Functional-structural plant modelling: a new versatile tool in crop science. J Exp Bot **61:** 2101–2115

Werner C, Ryel RJ, Correia O, Beyschlag W (2001) Effects of photoinhibition on whole-plant carbon gain assessed with a photosynthesis model. Plant Cell Environ **24:** 27–40

Wu C (2011) VisualSFM: A Visual Structure from Motion System. http://ccwu.me/vsfm/ (June 11, 2014)

Zhu XG, Ort DR, Whitmarsh J, Long SP (2004) The slow reversibility of photosystem II thermal energy dissipation on transfer from high to low light may cause large losses in carbon gain by crop canopies: a theoretical analysis. J Exp Bot **55:** 1167–1175